Biosensors and Bioelectronics 191 (2021) 113422

Contents lists available at ScienceDirect

Biosensors and Bioelectronics

journal homepage: www.elsevier.com/locate/bios

Functionalized europium-porphyrin coordination polymer: Rational design of high performance electrochemiluminescence emitter for mucin 1 sensing

Qian Han [a,b], Cun Wang [a,c], Pingkun Liu [a], Gui Zhang [a], Li Song [a], Yingzi Fu [a,*]

[a] Key Laboratory of Luminescence Analysis and Molecular Sensing (Southwest University), Ministry of Education, School of Chemistry and Chemical Engineering, Southwest University, Chongqing, 400715, China
[b] Hebei Key Laboratory of Environment Change and Ecological Construction, College of Resources and Environment Science, Hebei Normal University, Shijiazhuang, Hebei, 050024, China
[c] Chongqing Collaborative Innovation Center for Functional Food, Chongqing University of Education, Chongqing, 400067, China

ARTICLE INFO

Keywords:
Electrochemiluminescence
Europium-porphyrin coordination polymer
Emitter
Mucin 1
Biosensor

ABSTRACT

The excellent characteristics of porphyrins have inspired widespread interest in electrochemiluminescence (ECL). However, the limited ECL intensity and poor stability of porphyrins in aqueous solution are still severely restricted further biological application. Here, we subtly synthesized a functionalized europium and 5,10,15,20-tetrakis (4-carboxyphenyl) porphyrin (TCPP) coordination polymer (Eu-PCP) by a one-step solvothermal method. In sharp contrast to the pristine TCPP, Eu-PCP showed a higher and more stable ECL red-light emission (673 nm) at low potential (−1.1 V, vs Ag/AgCl), which was 7.7-fold higher ECL intensity and 4.6-fold efficiency. In view of the crucial role of mucin 1 (MUC1) in tumor overexpression, it was selected as the target molecule. Combined with exonuclease III (Exo III)-assisted recycling amplification strategy, a ternary ECL biosensor was constructed for the MUC1 detection based on Eu-PCP as a satisfied ECL emitter, gold nanoparticles capped CeO_2 (CeO_2@Au) as the coreactant accelerator and peroxydisulfate as coreactant. Meanwhile, gold nanoparticles capped MnO_2 (MnO_2@Au) was used as the quenching probe to achieve a highly sensitive detection of MUC1. The proposed biosensor exhibited a wide linear range from 1 fg mL^{-1} to 10 ng mL^{-1} with a low limit of detection (0.32 fg mL^{-1}). By changing the corresponding target recognition DNA, this strategy could be expanded to detect other biomarkers.

1. Introduction

Porphyrins are widely presented in nature and organisms, which are generally regarded as the colors of life as they are crucial in life-determining processes (Mone et al., 2019). Porphyrins are structurally robust heterocyclic conjugated molecules with the rigid geometric structures, excellent optoelectronic capabilities and easily varied terminal functional groups (Chen et al., 2021; Deng et al., 2015b). Such characteristics make porphyrins ideal class of electrochemiluminescence (ECL) emitters (Tokel et al., 1972). However, the research on functionalized porphyrinic ECL emitters is still in its infancy and remains a challenging task (Pu et al., 2019; Zhang et al., 2020). Most raw water-soluble porphyrins are unable to produce strong and stable ECL signals in aqueous media, which undoubtedly limits their applications (Luo et al., 2015). Though porphyrins anchoring on various carrier, such as zeolitic imidazole framework-8 (Fang et al., 2020) and carbon-based materials (Deng et al., 2015a; Liu et al., 2020) have been reported to circumvent weaknesses, the limited amount of the ECL emitter on the carrier surface and mismatched size cause the luminescent reagents leakage and low utilization. Or it is required to obtain a strong ECL emission under an excessive potential (−2.0 V or 2.0 V etc), which will induce the irreversible oxidative damage of biological sample (Fang et al., 2020; Zhou et al., 2020). Therefore, the exploration of new porphyrinic ECL emitters with simple synthesis strategy, good biocompatibility, stable ECL intensity and high efficiency at low-potential has become the focus and core of research.

Lanthanide ions have attracted more and more attention due to their photoluminescence and strong coordination ability (Wei et al., 2020). Especially, europium (III) ions (Eu^{3+}) have large Stokes' shifts, narrow emission spectra and intra-configurational 4f-4f transitions. The ECL phenomena of several Eu^{3+} complexes in acetonitrile were reported by Richter and Bard, 1996 (Richter et al., 1996). Eu^{3+} as the coreactant

* Corresponding author.
E-mail address: fyzc@swu.edu.cn (Y. Fu).

https://doi.org/10.1016/j.bios.2021.113422
Received 25 April 2021; Received in revised form 3 June 2021; Accepted 7 June 2021
Available online 9 June 2021

accelerator was doped in gadolinium based nanomaterials to improve the ECL efficiency (Xue et al., 2019). Our research group also synthesized a lanthanide (Ce^{3+}) luminescent coordination polymer as a cathodic ECL emitter for microRNA-141 detection (Wang et al., 2020a). However, the polymer with a short reaction time (10 min) is easy to cause the structure collapse in complex test environment. Porphyrin-based coordination polymers have predominant applications in the chemical sensors (Zhao et al., 2019), drug delivery (Liu et al., 2018), catalysis (Wang et al., 2020b) and photoelectrocatalysis (He et al., 2018). However, the ECL performances of porphyrin-based coordination polymers with lanthanide ions as metal centers have rarely reported (Demel et al., 2013). In order to address the existing problems of porphyrinic ECL emitters, we attempted to synthesize a functionalized Eu-porphyrin coordination polymer (Eu-PCP) to achieve stable and enhanced ECL performance (Scheme 1A).

Mucin 1 (MUC1) produced by epithelial tissue, is a large transmembrane glycoprotein (Huang et al., 2020). Since the overexpression of MUC1 is associated with human malignancies containing colon, breast, ovarian and pancreatic cancer, it is considered to be a crucial biomarker for early cancer diagnosis (Liang et al., 2020). Therefore, the quantitative analysis of MUC1 by a simple, fast, sensitive and specific detection technique has become the pivotal.

In this regard, we synthesized europium chelated 5,10,15,20-tetrakis (4-carboxyphenyl) porphyrin (TCPP) coordination polymer (Eu-PCP) by a simple and reliable solvothermal method (Scheme 1A). Using peroxydisulfate ($S_2O_8^{2-}$) solution as coreactant, Eu-PCP achieved a high and stable ECL red-light emission (673 nm) at low-potential (−1.1 V vs Ag/AgCl). Eu-PCP was employed as a satisfied emitter to establish a ternary ECL biosensor for sensitive detection of MUC1 with the help of exonuclease III (Exo III)-assisted target recycling amplification strategy. Gold nanoparticles (Au NPs) capped CeO_2 (CeO_2@Au) was used as a coreactant accelerator to promote the ECL reaction, and matrix to catch the capture hairpin DNA 1 (HP1). Au NPs capped MnO_2 (MnO_2@Au) as a quencher was labeled with hairpin DNA 3 (MnO_2@Au-HP3). When MUC1 was introduced to trigger the target recycling amplification, vast target substitutes (MnO_2@Au–S1) were output, eventually achieving a quenched signal for the detection of MUC1 at low levels. The proposed ECL biosensor achieves a highly selective and sensitive detection of MUC1 at low-potential that provides a new opportunity for the development of various cancer biomarker biosensors.

2. Experimental section

2.1. Materials and reagents

5,10,15,20-tetrakis (4-carboxyphenyl) porphyrin (TCPP), europium nitrate hexahydrate ($Eu(NO_3)_3{\cdot}6H_2O$), zinc acetate dihydrate ($Zn(CH_3COO)_2{\cdot}2H_2O$), potassium persulfate ($K_2S_2O_8$, 99.99%), cerium nitrate hexahydrate ($Ce(NO_3)_3{\cdot}6H_2O$), dimethyl formamide (DMF), sodium citrate and urea were purchased from Aladdin Biochemical Technology Co. Ltd (Shanghai, China). Gold chloride tetrahydrate ($HAuCl_4{\cdot}4H_2O$), sodium borohydride ($NaBH_4$), poly-(diallyldimethylammoniumchloride) (PDDA), 6-mercaptohexanol (MCH) and tris(hydroxymethyl)aminomethane hydrochloride (Tris-HCl) were

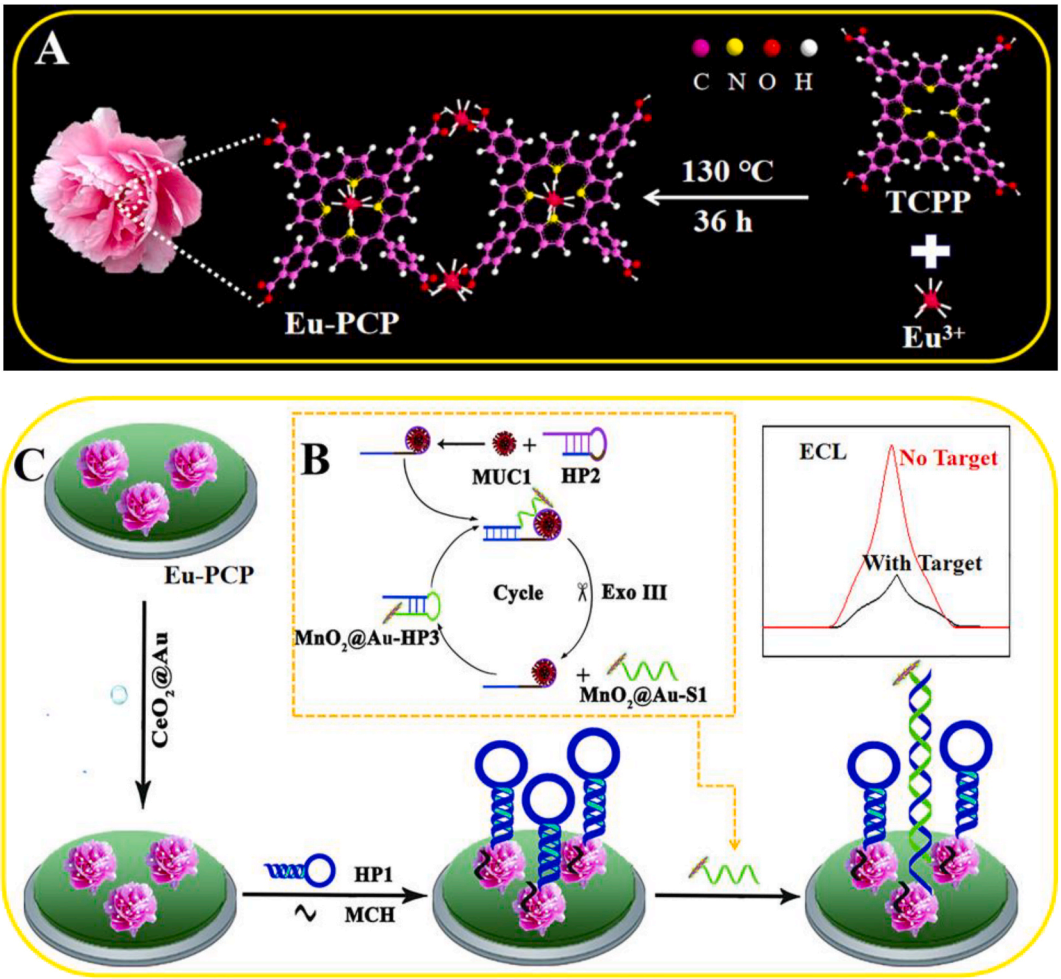

Scheme 1. Schematic illustration of (A) the synthesis of Eu-PCP, (B) Exo III-assisted recycling amplification strategy and (C) the preparation of the ECL sensor for target MUC1 detection.

provided by Sigma-Aldrich Co. (St. Louis, MO, USA). Human mucin 1 (MUC1) was provided by North Connaught Biotechnology (Shanghai, China). Exonuclease III (Exo III) and the HPLC-purified oligonucleotides in this work were obtained from Sangon Biotech Co. Ltd. (Shanghai, China). All sequences of the oligonucleotides are listed as follows: the hairpin DNA 1 (HP1): 5′–SH–TTT TTT GGT ATT ATT CGC CCA AGT AAT AAT ACC CTG GCC-3′; HP2: 5′-CGT GTG GCC AGG GTA TCC AGC TCA TTT GCA GTT GAT CCTTTG GAT ACC CTG GTT TTT-3′; HP3: 5′–NH_2–GGC CAG GGT ATT ATT ACT TTT GCC GAT ACC CTG GCC ACA CG-3′. Each hairpin DNA was heated to 95 °C for 5 min and slowly cooled to room temperature at a rate of 1 °C·min^{-1} for annealing. In addition, 0.1 mol L^{-1} Tris-HCl buffer (pH 7.4, containing 140 mmol L^{-1} NaCl, 5 mmol L^{-1} KCl, and 1 mmol L^{-1} $MgCl_2$) was employed for DNA hybridization and stock solutions. The 0.1 mol L^{-1} phosphate-buffered saline (PBS, pH 7.4) for ECL experiment was composed of 0.1 mol L^{-1} Na_2HPO_4, 0.1 mol L^{-1} KH_2PO_4 and 0.1 mol L^{-1} KCl. All solutions were prepared using ultrapure water (18.2 MΩ·cm).

2.2. Apparatus

The ECL and electrochemical measurements were performed on a model MPI-E electrochemiluminescence analyzer (Xi'an Remex Analysis Instruments Co. Ltd. Xi'an, China) and a CHI 604D electrochemistry workstation (Shanghai Chenhua Instruments Co, China), respectively. A standard three-electrode system was composed of a bare or modified glassy carbon electrode (GCE, $\Phi = 4$ mm) as the working electrode, an Ag/AgCl as reference electrode and a Pt wire as counter electrode. All measurements were carried out at the room temperature of 25 ± 1 °C. The other apparatus are described in the Supporting Information.

2.3. Synthesis of Eu-PCP

Eu-PCP was synthesized by previous method with slight changes (Demel et al., 2013). 2.4 mg TCPP was dissolved in 6 mL of DMF under stirring. 6 mmol of $Eu(NO_3)_3{\cdot}6H_2O$ (5.3 mg) was added and formed dark red solution. After stirring for 15 min, the above solution was transferred into a teflon-lined stainless steel autoclave, and heated at 130 °C for 36 h. After the reaction, the precipitate was centrifuged and washed three times. Finally, the cleaned precipitate was dried at 60 °C and redispersed in ultrapure water (1 mg mL^{-1}) for further use. As control, the other two Eu-PCP with different solvent volume ratios (V_{DMF}:$V_{ethanol}$ = 1:1 and V_{DMF}:$V_{ethanol}$ = 0:1) were synthesized by the same methods. The TCPP was initially dissolved in DMF solution to obtain TCPP monomer, and TCPP aggregates was prepared by the reprecipitation procedure (Doan et al., 2005).

2.4. Synthesis of CeO_2@Au and MnO_2@Au

First, CeO_2 nanospheres and MnO_2 nanorods were prepared by a one-pot hydrothermal method (Lin et al., 2020; Zuo et al., 2019). Negatively charged gold nanoparticles (Au NPs) were prepared according to the literature methods (Hu et al., 2019). Then 1 mg CeO_2 was dispersed in 2 mL of PDDA solution (1%), which was a cationic polyelectrolyte polymeric material to make CeO_2 with positive charge. Subsequently, the mixture was centrifuged, and 2 mL of Au NPs dispersion was added. After incessant stirring for 3 h, the resultant composites CeO_2@Au was obtained through the oppositely charged interaction between CeO_2 and Au NPs. MnO_2@Au was prepared using the same method.

2.5. Output the quencher probes by exo III-assisted recycling

The preparation of MnO_2@Au labeled HP3 (MnO_2@Au-HP3) was as follows: HP3 (200 μL, 2 μmol L^{-1}) with an amino at its 5′-end was mixed with MnO_2@Au suspension (200 μL, 1 mg mL^{-1}) to get MnO_2@Au-HP3 by Au–N bond. After shaking gently for 12 h, the above mixture was centrifuged to remove the excess HP3 and was stored at 4 °C for further use.

10 μL of HP2 (1 μmol L^{-1}), 10 μL of MnO_2@Au-HP3 (1 μmol L^{-1}), 20 μL of Exo III (1 U/μL) and 10 μL of different concentrations of MUC1 were mixed to form HP2-MUC1-MnO_2@Au-HP3 complex, and incubated at 37 °C for 90 min to output the quencher probes (MnO_2@Au–S1) (Scheme 1B). With the existence of Exo III, the resultant HP2-MUC1-MnO_2@Au-HP3 complex was cleaved and released massive target substitutes, MnO_2@Au–S1. Meanwhile, the released MUC1 and HP2 complex could further hybridize with other complementary MnO_2@Au-HP3 and repeat the above cleaving processes. Finally, the products were heated at 80 °C for 10 min to inactivate Exo III and reserved at 4 °C.

2.6. Assembly of the biosensor

Prior to use, the GCE was polished carefully and cleaned (Liu et al., 2020). As depicted in Scheme 1C, the prepared Eu-PCP suspension (1 mg mL^{-1}) was deposited onto the cleaned GCE surface to form a homogeneous layer (Eu-PCP/GCE). Then CeO_2@Au was added onto the above modified electrode (CeO_2@Au/Eu-PCP/GCE). Subsequently, HP1 solution (10 μL, 1 μmol L^{-1}) was incubated overnight on the modified GCE surface by Au–S bond (HP1/CeO_2@Au/Eu-PCP/GCE). After the HP1/CeO_2@Au/Eu-PCP/GCE was further blocked with MCH (MCH/HP1/CeO_2@Au/Eu-PCP/GCE), the above output quencher probes (MnO_2@Au–S1) were dropped onto the electrode surface and incubated at 37 °C for 2 h. Through base complementary pairing principle, MnO_2@Au–S1 was able to spontaneously hybridize with HP1, leading to a decreased ECL signal.

For the detection of MUC1 by ECL measurement, the photomultiplier tube voltage was set at 800 V, and the scanning potential was from 0.0 to −1.1 V with a scan rate of 200 mV s^{-1}. The ECL detection was performed in 10 mmol L^{-1} $S_2O_8^{2-}$ solution (0.1 mol L^{-1} PBS, pH 7.4).

3. Results and discussion

3.1. Materials characterization

The morphologies of the TCPP monomer and as-prepared Eu-PCP were characterized and compared by scanning electron microscopy (SEM). As shown in Fig. 1A and B, the TCPP monomer displays a clear net structure, while the Eu-PCP exhibits a peony flower-like morphology consisting of a large-scale 2D nanosheets. The dark-field high-magnification transmission electron microscopy (TEM) image further confirms the structure of Eu-PCP (Fig. 1C). The TEM mapping and energy dispersive X-ray (EDX) of Eu-PCP indicate the uniform distribution and the percentage of C, N, O and Eu elements (Fig. 1D and Fig. S1). Fig. S2A displays 2D atomic force microscope (AFM) image of Eu-PCP with a thickness value of 398.9 nm, and Eu-PCP-coated surface has an average roughness of 100.3 nm. As illustrated in Fig. 1E, the SEM image of CeO_2@Au nanocompsites demonstrates that CeO_2 is spherical particle and Au NPs has been successfully attached to the CeO_2 modified surface. The EDX of CeO_2@Au shows that the element percentage of Ce, O and Au (Fig. S3). In addition, Fig. 1F depicts the Au NPs are uniformly distributed on the rod-like MnO_2 surface.

The Fourier transform infrared (FTIR) spectra of TCPP monomer and Eu-PCP are analyzed in Fig. 2B. The strong C═O stretching band of TCPP monomer is at 1590 cm^{-1}, while the skeleton vibrations at 1534 cm^{-1}, 1400 cm^{-1}, and 1023 cm^{-1} are observed in original TCPP (curve a). The broad bands (2924 cm^{-1}, 2964 cm^{-1}, 3393 cm^{-1}) belong to the O–H and N–H stretching vibration (Zhou et al., 2020). But for Eu-PCP, the characteristic absorption peaks of C═O have red-shifted and appeared at about 1600 cm^{-1} and 1692 cm^{-1}. The stretching vibrations of O–H and N–H are all diminution, which indicates the formation of coordination bonds between Eu^{3+} and TCPP (curve b). Different from the spectra of TCPP monomer and $Eu(NO_3)_3$, the UV–vis spectrum of Eu-PCP displays an obvious red-shifted Soret band (431 nm) and four weak Q bands (525, 558, 594 and 652 nm) (Fig. 2B), that is mainly

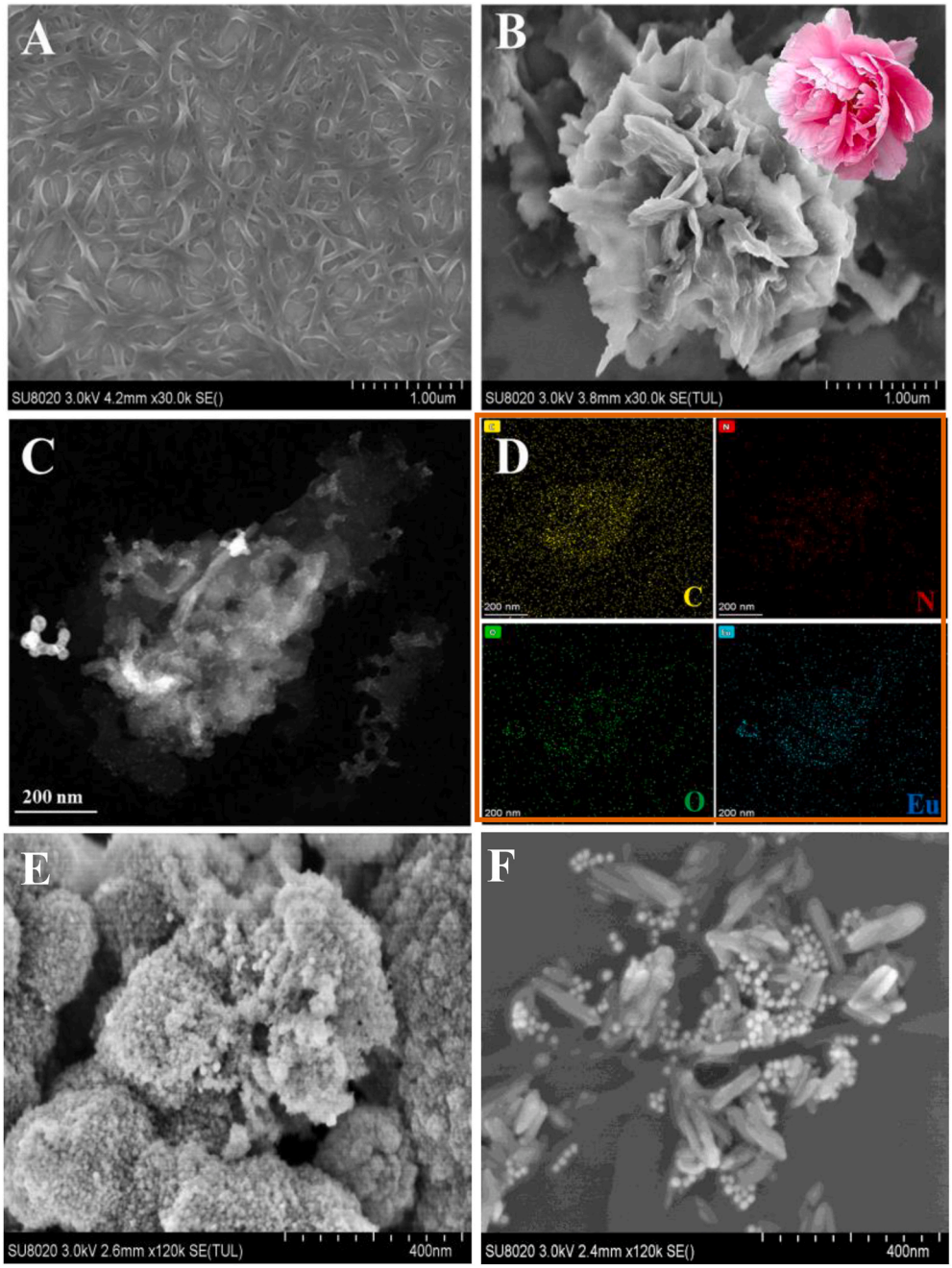

Fig. 1. SEM images of (A) TCPP monomer and (B) Eu-PCP. (C) Dark-field TEM image and (D) relative elemental mapping of C, N, O, Eu of Eu-PCP. SEM images of (E) CeO_2@Au and (F) MnO_2@Au.

resulted by the good electron-hole separation ability and photon absorption of Eu-PCP under light radiation (Ma et al., 2021). From the onset absorption peak, the optical band gap (Eg) of Eu-PCP was calculated (Eg = 1.88 eV) by Tauc plots (Fig. S4A) (Liu et al., 2019). Furthermore, the energy level of Eu-PCP was measured by cyclic voltammetry (CV) (Fig. S4B). From the onset of this oxidation peak (+0.66 V) and band gap (1.88 eV), the highest occupied molecular orbital (HOMO) and the lowest unoccupied molecular orbital (LUMO) levels were calculated as −5.02 eV and −3.14 eV, respectively (Gagne et al., 1980). The N_2 adsorption/desorption isotherm expressly reveals that the specific surface area of Eu-PCP is 101.00 $m^2\ g^{-1}$ (Fig. 2C), and the pore size of Eu-PCP is about 1.27 nm–2.5 nm, indicating the formation of a microporous framework. The X-ray diffraction (XRD) of TCPP powder confirms that the structure is disordered and amorphous (Fig. 2D, curve a). For Eu-PCP, the peaks at $2\theta = 5.39°$, 7.58°, and 10.64° are indexed to the (020), (021) and (041) planes, respectively (curve b). The X-ray photoelectron spectroscopy (XPS) analysis of Eu-PCP is presented in Fig. S5A to S5E. The full survey spectrum of Eu-PCP manifests the existence of C, N, O and Eu elements (Fig. S5A). Especially, the peaks of Eu3d at binding energy of 1135.19 eV and 1164.59 eV are ascribed to the $Eu3d^5$ and $Eu3d^3$ of Eu–O bond, and two peaks at 1137.06 eV and 1166.85 eV are separately attributed to $Eu3d^5$ and $Eu3d^3$ of Eu–N bond, which powerfully demonstrates the coordination interaction between Eu^{3+} and TCPP (Fig. S5E).

3.2. ECL behavior of Eu-PCP

As presented in Fig. 3A, the ECL behavior of the prepared Eu-PCP

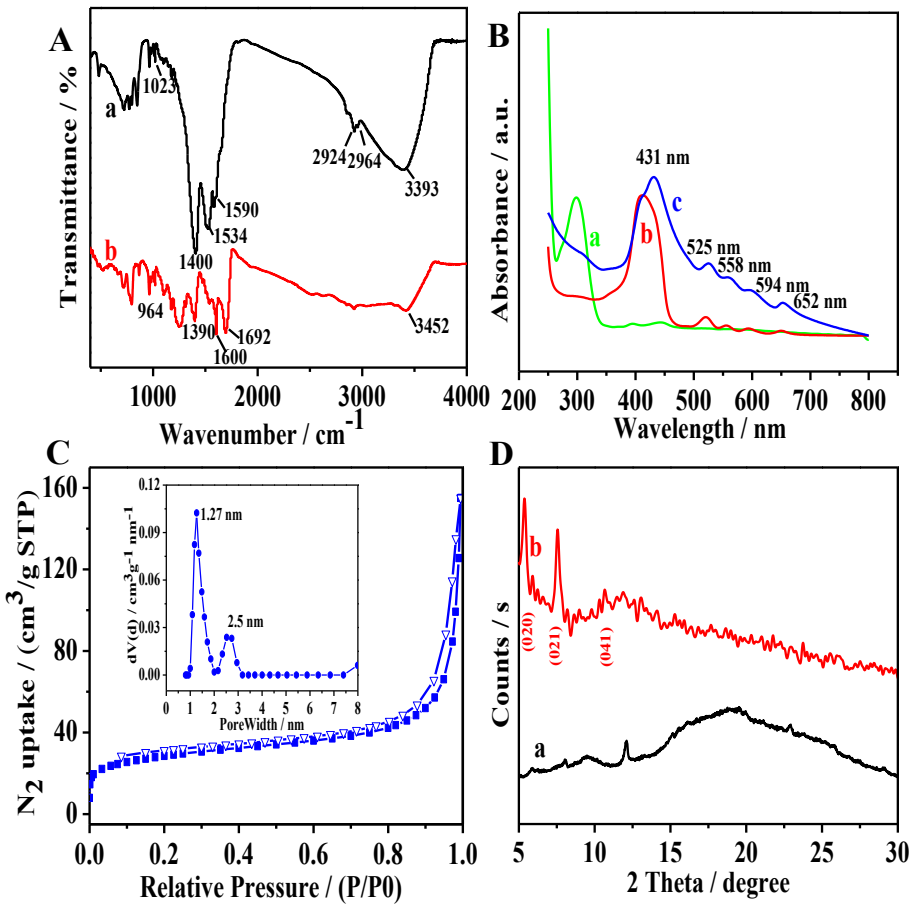

Fig. 2. (A) FTIR spectra of (a) TCPP and (b) Eu-PCP. (B) UV–vis absorption spectra of (a) $Eu(NO_3)_3$, (b) TCPP and (c) Eu-PCP. (C) Nitrogen adsorption and desorption isotherms measurment of Eu-PCP at 77 K (inset: pore size distribution graph). (D) XRD pattern of (a) TCPP and (b) Eu-PCP.

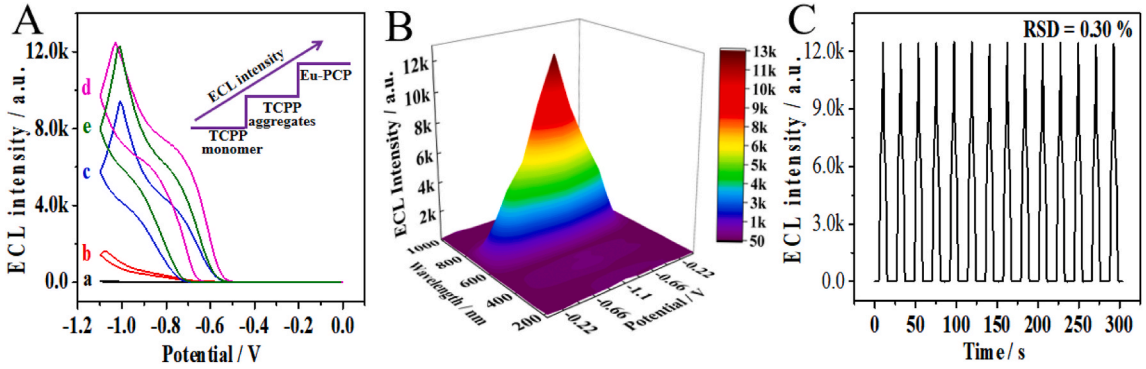

Fig. 3. (A) ECL-potential profiles of different modified electrodes in 10 mmol L^{-1} $S_2O_8^{2-}$ solution: (a) bare GCE, (b) TCPP monomer/GCE, (c) TCPP aggregates/GCE, (d) Eu-PCP/GCE, (e) Eu-PCP/GCE (in N_2). (B) The 3D ECL-potential-wavelength image of the Eu-PCP/GCE in $S_2O_8^{2-}$ solution. (C) The ECL responses of Eu-PCP/GCE with $S_2O_8^{2-}$ as coreactant under consecutive scans for 300s.

was investigated by comparison experiments. The ECL curves of the modified electrodes by TCPP monomer (TCPP monomer/GCE), TCPP aggregates (TCPP aggregates/GCE), and Eu-PCP (Eu-PCP/GCE) were measured in 10 mmol L^{-1} $S_2O_8^{2-}$ solution (0.1 mol L^{-1} PBS, pH 7.4). A weak ECL response is observed on bare GCE (curve a). The ECL signal of TCPP monomer/GCE is 1625 a.u. (curve b) while TCPP aggregates/GCE displays an increased ECL signal (9428 a.u. curve c). Evidently, the ECL intensity of the Eu-PCP/GCE reaches up to 12,477 a.u. (curve d), which is 7.7 times higher than that of the TCPP monomer/GCE. The ECL efficiency of Eu-PCP is enhanced 4.6-fold (Section S7, Supporting Information). Such enhanced ECL intensity of Eu-PCP is due to the reduced band gap which increases the electron-hole recombination efficiency, and rigid coordination ploymer that effectively suppresses the non-radiative transition. The effect of dissolved O_2 on the ECL response was investigated by comparing the signals before and after blowing high purity N_2 in Eu-PCP-$S_2O_8^{2-}$ system. No obvious change of ECL intensity is obtained after removing O_2 (curve e), indicating that the effect of dissolved O_2 in Eu-PCP-$S_2O_8^{2-}$ system can be negligible. The three-dimensional (3D) ECL-potential-wavelength image of the Eu-PCP shows a maximum ECL emission wavelength at 673 nm, proving that the Eu-PCP is an ECL red-light emitter (Fig. 3B). Fig. 3C shows the ECL responses of Eu-PCP with the potential window from 0.0 to −1.1 V after

300 s measurements. The relative standard deviation (RSD) is only 0.30%, suggesting a superior stability and application potential of Eu-PCP.

As control, the ECL performance of Eu-PCP synthesized with different solvent ratios (V_{DMF}:$V_{ethanol}$ = 1:1 and 0:1) were investigated. The SEM image of Eu-PCP (V_{DMF}:$V_{ethanol}$ = 1:1) displays a coexistence of flaky and granular structures (Fig. S6A). While the Eu-PCP (V_{DMF}:$V_{ethanol}$ = 0:1) exhibits a nonstandard granular structure (Fig. S6B). The ECL signals of them are all weak in the studied potential window (Fig. S6C and D), mainly because the unstable framework structure formed in inappropriate solvent ratios affects the ECL intensity.

3.3. Exo III-assisted recycling amplification principle

For improving the sensitivity of the biosensor, Exo III was employed to execute the target recycling amplification strategy (Scheme 1B). When target MUC1 was introduced, the hairpin DNA 2 (HP2) could be opened. The exposed DNA fragment can complement with MnO_2@Au-HP3 to form the MnO_2@Au labeled DNA-MUC1 complex. While the Exo III would specifically catalyze stepwise digestion of a DNA duplex from the 3′-blunt end, and output the target substitutes (MnO_2@Au–S1). The HP2-MUC1 complex was released again that can bind the next MnO_2@Au-HP3 to repeat the cycle. After the cycle was terminated, MnO_2@Au–S1 was introduced on the modified electrode, it could hybridized with HP1 to cause a remarkable ECL "signal off" state for sensitively detecting MUC1.

3.4. EIS and ECL characterizations of the stepwise modified electrodes

Fig. 4A exhibits the electrochemical impedance spectroscopy (EIS) of stepwise process of electrode modification. The charge-transfer resistance (R_{et}) of bare GCE is very small (curve a), while the R_{et} of Eu-PCP/GCE is remarkably increased (curve b). After coating CeO_2@Au composites onto the Eu-PCP/GCE, the R_{et} of CeO_2@Au/Eu-PCP/GCE (curve c) is reduced, indicating that CeO_2@Au has a good conductivity. With the stepwise assembling of capture DNA (curve d) and MCH (curve e), R_{et} is increased in sequence, since the negatively charged DNA and MCH can greatly prevent the electron transfer of $[Fe(CN)_6]^{3-/4-}$. After the incubation of MnO_2@Au–S1, the R_{et} is increased obviously (curve f). The weak conductivity of MnO_2@Au–S1 weakens the electron transfer ability. The ECL responses of different modified electrodes were also investigated to characterize the construction process (Fig. 4B). Compared with that of bare GCE, the ECL response has been enhanced significantly on the Eu-PCP/GCE (curve b). Then, the ECL signal of CeO_2@Au/Eu-PCP/GCE is further increased (curve c). The strong ECL response is ascribed to the fact that CeO_2 as a coreactant accelerator can promote the ECL reaction and electronic transfer between $S_2O_8^{2-}$ and Eu-PCP. However, when the HP1 and MCH were successively incubated on the CeO_2@Au/Eu-PCP/GCE surface, a reduced ECL response was obtained (curve d and e). After the MnO_2@Au–S1 was incubated, a significantly declined ECL signal (curve f) was gotten, attributing to the quenching effect of MnO_2@Au. The results of EIS and ECL measurements proved the successful construction of the proposed biosensor.

3.5. Optimization of the assay conditions

As shown in Fig. 4C, the influence of pH from 6.0 to 9.0 was investigated. The corresponding ECL intensity decreased with the increasing of pH, and reached a lowest ECL intensity at pH 7.4. Then, a slightly changes after pH 7.4 were observed. Thus, pH 7.4 was chosen as the optimized pH condition. Besides, the incubation time of MnO_2@Au–S1 plays a crucial role in the quenching effect (Fig. 4D). The ECL intensity was consecutively decreased with the increase of incubation time. Until the time reached at 120 min, the ECL intensity tended to a platform. In order to achieve a good quenching effect under a suitable time, the optimum incubation time of the MnO_2@Au–S1 was selected as 120 min.

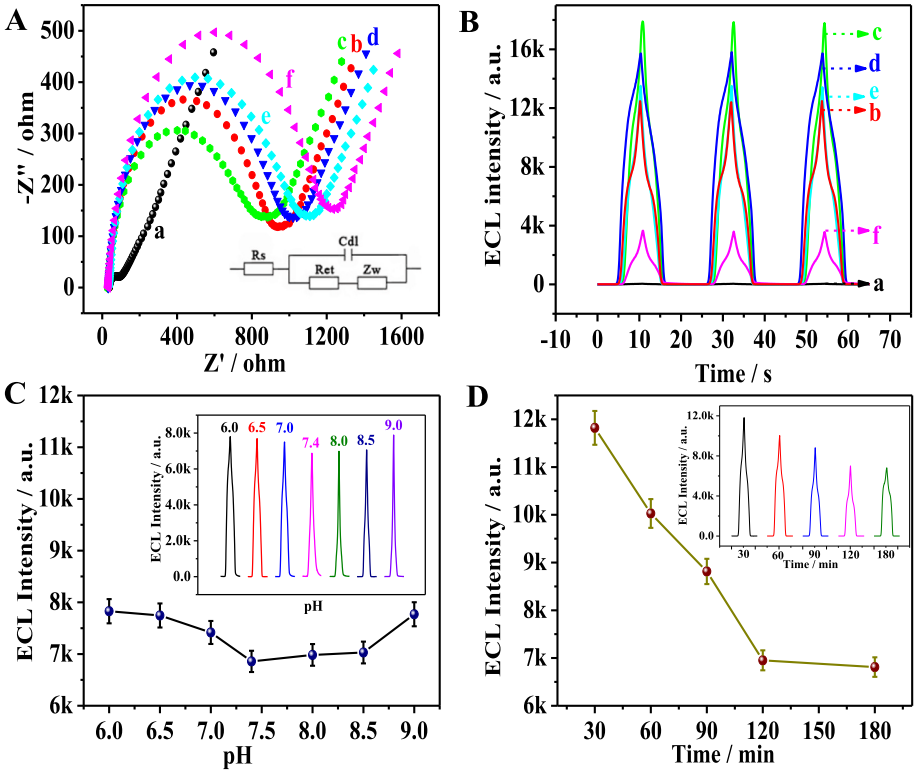

Fig. 4. (A) EIS profiles (inset: equivalent circuit) and (B) ECL-time curves of stepwise-modified electrodes: (a) bare GCE, (b) Eu-PCP/GCE, (c) CeO_2@Au/Eu-PCP/GCE, (d) HP1/CeO_2@Au/Eu-PCP/GCE, (e) MCH/HP1/CeO_2@Au/Eu-PCP/GCE, (f) MnO_2@Au–S1/MCH/HP1/CeO_2@Au/Eu-PCP/GCE. The effects of (C) pH and (D) the incubation time of MnO_2@Au–S1 (inset: the ECL response corresponding to each condition).

3.6. Assay performance for detection of MUC1

The ECL behaviors of the prepared biosensor were explored towards different concentration of MUC1 under optimum condition. The ECL responses are dependent on the increased concentrations of MUC1 varying from 1 fg mL^{-1} to 10 ng mL^{-1} (Fig. 5A). A good quantitatively linear relationship between ECL signals (I) and the logarithm concentrations of MUC1 (lgc) is obtained in Fig. 5B. The linear equation is I (a.u.) = −10212.98–1550.06 lgc (R^2 = 0.993). Additionally, the proposed biosensor exhibits a wider detection range and a relatively lower limit of detection (LOD, 0.32 fg mL^{-1}) in comparison with previous reports (Table 1), indicating the good performances of this sensor in MUC1 detection.

Table 1
Comparison of different methods for the detection of MUC1.

Analytical methods	Linear range	Detection limit	References
ECL	0.05 pg mL^{-1} - 10 ng mL^{-1}	0.05 pg mL^{-1}	Liang et al. (2020)
ECL	10 fg mL^{-1} - 1 ng mL^{-1}	5.8 fg mL^{-1}	Zhou et al. (2019)
FL	0.01–5 nM	3.33 pmol L^{-1} (1 ng mL^{-1})	Ma et al. (2016)
FL	1 pg mL^{-1} - 20 ng mL^{-1}	0.23 pg mL^{-1}	Yang et al. (2018)
ECL	1 fg mL^{-1} - 1 ng mL^{-1}	0.49 fg mL^{-1}	Huang et al. (2020)
ECL	1 fg mL^{-1}-10 ng mL^{-1}	0.32 fg mL^{-1}	this work

3.7. Selectivity, reproducibility and stability

The selectivity of the prepared biosensor was investigated by incubating with various possible interferences, including bovine albumin (BSA), alpha fetoprotein (AFP), human serum albumin (HSA), prostate specific antigen (PSA) and hemoglobin (Hb) with a 10-fold higher concentration (10 ng mL^{-1}) than that of MUC1 (1 ng mL^{-1}). The ECL intensity of the interfering substances were no any noticeable change (Fig. 5C). However, after the mixture including MUC1 and other interferences was incubated, the ECL signal greatly decreased, which was approached to that of MUC1 (1 ng mL^{-1}). Meanwhile, the reproducibility was assessed through intra- and inter-assays for the MUC1 detection (1 ng mL^{-1}) (Fig. S7). The intra-assay was estimated using the seven modified electrodes in identical environment, the relative standard deviation (RSD) was calculated to be 1.8%. The RSD of inter-assay on seven batches biosensor was 2.1%. The repeatability was investigated based on five repetitive measurements, and the RSD was 3.9%. All results indicated a good reproducibility and repeatability of the proposed biosensor. Subsequently, the stability of the biosensor has been investigated by detection of MUC1 (1 pg mL^{-1}) with continuous scanning of 300s (Fig. 5D). A low RSD (0.67%) reveals that the proposed biosensor possesses a satisfied stability.

3.8. ECL mechanism

The possible ECL mechanism of the Eu-PCP-$S_2O_8^{2-}$ system were identified via ECL spectroscopy (Fig. S8A). The ECL spectrum of Eu-PCP/GCE in $S_2O_8^{2-}$ solution shows an obviously emission peaks at

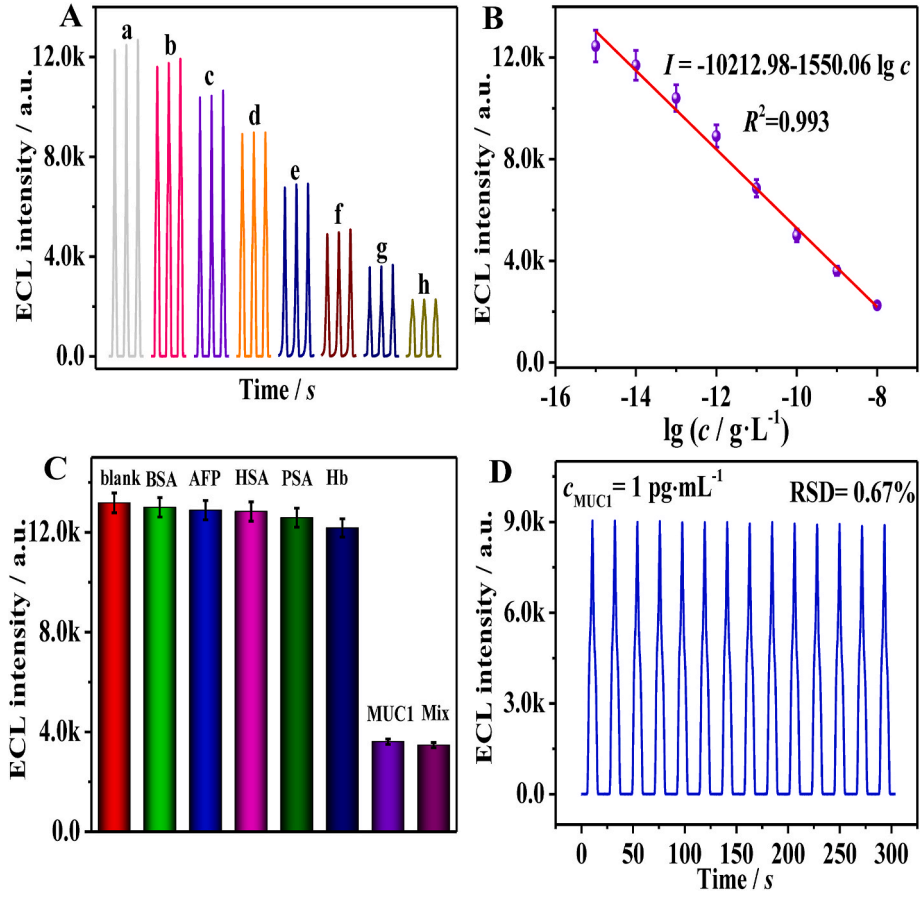

Fig. 5. (A) ECL responses and (B) calibration curves for different concentrations of MUC1 (from a to h): 1 fg mL^{-1}, 10 fg mL^{-1}, 100 fg mL^{-1}, 1 pg mL^{-1}, 10 pg mL^{-1}, 100 pg mL^{-1}, 1 ng mL^{-1}, 10 ng mL^{-1}. (C) Selectivity of the ECL biosensor for different targets from left to right: blank sample, 10 ng mL^{-1} of BSA, AFP, HSA, PSA and Hb, 1 ng mL^{-1} of MUC1 and the mixture sample. (D) Stability of the proposed ECL sensor under consecutive scans for 300 s (c_{MUC1} = 1 pg mL^{-1}).

673 nm (curve a). The ECL intensity of CeO_2@Au/Eu-PCP/GCE has been enhanced without any significant change in spectral position (curve b), which further demonstrates that the ECL emitter is Eu-PCP and the CeO_2@Au acts as a robust coreaction accelerator in the Eu-PCP-$S_2O_8^{2-}$ system. Subsequently, the ECL spectrum of MnO_2@Au/CeO_2@Au/Eu-PCP/GCE shows that the emission peak is at 676 nm, while the ECL intensity is declined indicating the effective quenching-effect of MnO_2@Au (curve c). The ECL mechanism of Eu-PCP-$S_2O_8^{2-}$ system is summarized as follows:

$$S_2O_8^{2-} + e^- \rightarrow SO_4^{2-} + SO_4^{-\bullet} \quad (1)$$

$$\text{Eu-PCP} + e^- \rightarrow \text{Eu-PCP}^{-\bullet} \quad (2)$$

$$\text{Eu-PCP}^{-\bullet} + SO_4^{-\bullet} \rightarrow SO_4^{2-} + \text{Eu-PCP}^* \quad (3)$$

$$\text{Eu-PCP}^* \rightarrow \text{Eu-PCP} + h\nu \quad (4)$$

To confirm the quenching effect of MnO_2@Au toward the Eu-PCP-$S_2O_8^{2-}$ system, the UV–vis absorption of MnO_2@Au and ECL spectrum of Eu-PCP have been investigated in Fig. S8B. The wide UV–vis absorption spectrum of MnO_2@Au has a suitable overlap with the ECL emission spectrum of Eu-PCP, suggesting a possible resonant energy transfer between Eu-PCP (donor) and MnO_2@Au (acceptor).

3.9. Real samples application

The feasibility of the fabricated biosensor in practice was estimated by recovery experiments. A certain concentration of MUC1 solution (0.1 pg mL^{-1}, 0.1 ng mL^{-1} and 1 ng mL^{-1}) in healthy human serum samples (100-fold diluted by PBS) was detected. The recovery was in the range of 99.0–108.0%, and the RSD varied from 1.0% to 1.4% (Table S1), implying an acceptable practical applicability.

4. Conclusions

It is worth highlighting that the new synthetic Eu-PCP with porosity and biocompatibility displays a good stability and enhanced ECL efficiency at low-potential with $S_2O_8^{2-}$ as coreactant due to the narrow band gap (1.88 eV) and a well-ordered coordination array. The CeO_2@Au as the coreactant accelerator can efficiently promote more $SO_4^{-\bullet}$ to react with the oxidation process of Eu-PCP. Meanwhile, MnO_2@Au as a quencher exhibits a good quenching effect, achieving sensitive detection of MUC1. Significantly, the proposed ternary ECL biosensor not only gives a low LOD (0.32 fg mL^{-1}) toward MUC1, but also opens a new way for highly sensitive and selective detection of biomarkers in disease diagnosis and clinical analysis.

CRediT authorship contribution statement

Qian Han: Conceptualization, Methodology, Investigation, Writing – original draft, Visualization. **Cun Wang:** Data curation, Resources, Investigation. **Pingkun Liu:** Data curation. **Gui Zhang:** Formal analysis. **Li Song:** Validation. **Yingzi Fu:** Writing – review & editing, Supervision, Project administration, Funding acquisition.

Declaration of competing interest

The authors declare that they have no known competing financial interests or personal relationships that could have appeared to influence the work reported in this paper.

Acknowledgments

This work was supported by the National Natural Science Foundation of China (No. 21272188, 22077105), the Natural Science Foundation Project of Chongqing City (cstc2020jcyj-msxmX0854) and the Science and Technology Project of Hebei Education Department (QN2020123).

Appendix A. Supplementary data

Supplementary data to this article can be found online at https://doi.org/10.1016/j.bios.2021.113422.

References

Chen, J.J., Zhu, Y.F., Kaskel, S., 2021. Angew. Chem. Int. Ed. 60, 5010–5035.
Demel, J., Kubát, P., Millange, F., Marrot, J., Císařová, I., Lang, K., 2013. Inorg. Chem. 52, 2779–2786.
Deng, S.Y., Yuan, P.X., Ji, X.B., Shan, D., Zhang, X.J., 2015a. ACS Appl. Mater. Interfaces 7, 543–552.
Deng, S.Y., Zhang, T.T., Ji, X.B., Wan, Y., Xin, P., Shan, D., Zhang, X.J., 2015b. Anal. Chem. 87, 9155–9162.
Doan, S.C., Shanmugham, S., Aston, D.E., McHale, J.L., 2005. J. Am. Chem. Soc. 127, 5885–5892.
Fang, Y., Wang, H.M., Gu, Y.X., Yu, L., Wang, A.J., Yuan, P.X., Feng, J.J., 2020. Anal. Chem. 92, 3206–3212.
Gagne, R.R., Koval, C.A., Lisensky, G.C., 1980. Inorg. Chem. 19, 2854–2855.
He, T., Chen, S.M., Ni, B., Gong, Y., Wu, Z., Song, L., Gu, L., Hu, W.P., Wang, X., 2018. Angew. Chem. Int. Ed. 57, 3493–3498.
Hu, Q.Y., Yang, J.Y., Zheng, Z.Y., Ding, Y.P., Chen, Y.W., Gao, W.H., 2019. Biosens. Bioelectron. 143, 111627.
Huang, W., Hu, G.B., Yao, L.Y., Yang, Y., Liang, W.B., Yuan, R., Xiao, D.R., 2020. Anal. Chem. 92, 3380–3387.
Liang, Z.H., Liu, Y., Zhang, Q., Guo, Y.P., Ma, Q., 2020. Chem. Eng. J. 385, 123825.
Lin, Y., Zhang, L., Xiao, J.Y., Liu, H.D., 2020. Sustain. Energ Fuels 4, 633–642.
Liu, M., Wang, L., Zheng, X.H., Liu, S., Xie, Z.G., 2018. ACS Appl. Mater. Interfaces 10, 24638–24647.
Liu, Y.Q., Wang, L., Feng, H.X., Ren, X.T., Ji, J.J., Bai, F., Fan, H.Y., 2019. Nano Lett. 19, 2614–2619.
Liu, G., Hong, J.J., Ma, K.F., Wan, Y., Zhang, X.T., Huang, Y.Q., Kang, K., Yang, M., Chen, J.L., Deng, S.Y., 2020. Biosens. Bioelectron. 150, 111963.
Luo, D., Huang, B.M., Wang, L., Mahmoud idris, A., Wang, S.X., Lu, X.Q., 2015. Electrochim. Acta 151, 42–49. https://doi.org/10.1016/j.electacta.2014.11.004.
Ma, C., Liu, H.Y., Tian, T., Song, X.R., Yu, J.H., Yan, M., 2016. Biosens. Bioelectron. 83, 15–18.
Ma, J., Wang, W.J., Li, Y., Lu, Z.C., Tan, X.C., Han, H.Y., 2021. Anal. Chem. 93, 2090–2096.
Mone, M., Tang, S., Murto, P., Abdulahi, B.A., Larsen, C., Wang, J., Mammo, W., Edman, L., Wang, E.G., 2019. Chem. Mater. 31, 9721–9728.
Pu, G.Q., Yang, Z.F., Wu, Y.L., Wang, Z., Deng, Y., Gao, Y.J., Zhang, Z., Lu, X.Q., 2019. Anal. Chem. 91, 2319–2328.
Richter, M.M., Bard, A.J., 1996. Anal. Chem. 68, 2641–2650.
Tokel, N.E., Keszthelyi, C.P., Bard, A.J., 1972. J. Am. Chem. Soc. 94, 4872–4877.
Wang, C., Han, Q., Mo, F.J., Chen, M., Xiong, Z.W., Fu, Y.Z., 2020a. Anal. Chem. 92, 12145–12151.
Wang, B., Yang, F.L., Dong, Y.P., Cao, Y.Z., Wang, J.Y., Yang, B.J., Wei, Y., Wan, W.R., Chen, J.Z., Jing, H.W., 2020b. Chem. Eng. J. 396, 125255.
Wei, Y.P., Zhang, Y.W., Mao, C.J., 2020. J. Mater. Chem. B 8, 2471–2475.
Xue, J.W., Yang, L., Jia, Y., Wang, H., Zhang, N., Ren, X., Ma, H.M., Wei, Q., Ju, H.X., 2019. ACS Sens. 4, 2825–2831.
Yang, W.T., Shen, Y., Zhang, D.Y., Xu, W.J., 2018. Chem. Commun. 54, 10195–10198.
Zhang, Y.P., Zhao, Y.Q., Han, Z.G., Zhang, R.Z., Du, P.Y., Wu, Y.X., Lu, X.Q., 2020. Angew. Chem. Int. Ed. 59, 23261–23267.
Zhao, X., Bai, J., Bo, X.J., Guo, L.P., 2019. Anal. Chim. Acta 1075, 71–80.
Zhou, Y., Chai, Y.Q., Yuan, R., 2019. Anal. Chem. 91, 14618–14623.
Zhou, Y., He, J.L., Zhang, C.L., Li, J., Fu, X.X., Mao, W.R., Li, W.M., Yu, C., 2020. ACS Appl. Mater. Interfaces 12, 338–346.
Zuo, F.M., Zhang, C., Zhang, H., Tan, X.R., Chen, S.H., Yuan, R., 2019. Electrochim. Acta 294, 76–83.